# Indistinguishable photons from a single-photon device

**Charles Santori*, David Fattal*, Jelena Vučković*, Glenn S. Solomon*† & Yoshihisa Yamamoto*‡**

* *Quantum Entanglement Project, ICORP, JST, E. L. Ginzton Laboratory, Stanford University, Stanford, California 94305-4088, USA*
† *Solid-State Photonics Laboratory, Stanford University, Stanford, California 94305-4085, USA*
‡ *NTT Basic Research Laboratories, Atsugi, Kanagawa, 243-0198, Japan*

**Single-photon sources have recently been demonstrated using a variety of devices, including molecules[1–3], mesoscopic quantum wells[4], colour centres[5], trapped ions[6] and semiconductor quantum dots[7–11]. Compared with a Poisson-distributed source of the same intensity, these sources rarely emit two or more photons in the same pulse. Numerous applications for single-photon sources have been proposed in the field of quantum information, but most—including linear-optical quantum computation[12]—also require consecutive photons to have identical wave packets. For a source based on a single quantum emitter, the emitter must therefore be excited in a rapid or deterministic way, and interact little with its surrounding environment. Here we test the indistinguishability of photons emitted by a semiconductor quantum dot in a microcavity through a Hong–Ou–Mandel-type two-photon interference experiment[13,14]. We find that consecutive photons are largely indistinguishable, with a mean wave-packet overlap as large as 0.81, making this source useful in a variety of experiments in quantum optics and quantum information.**

When identical single photons enter a 50–50 beam splitter from opposite sides, quantum mechanics predicts that both photons must leave in the same direction, if their wave packets overlap perfectly. This two-photon interference effect originates from the Bose–Einstein statistics of photons. This bunching effect was first observed using pairs of highly correlated photons produced by parametric downconversion[14], but it should also occur with single, independently generated photons. Most proposed applications for single-photon sources in the field of quantum information (with the notable exception of quantum cryptography[15]) involve two-photon interference. Such applications include quantum teleportation[16], post-selective production of polarization-entangled photons[17], and linear-optics quantum computation[12]. It is therefore important to demonstrate that consecutive photons emitted by a single-photon source are identical and exhibit mutual two-photon interference effects.

The experiment described here used a semiconductor quantum dot as the photon source. Quantum dots are attractive as single-photon sources because they are relatively stable, have narrow spectral linewidths and rapid radiative decay rates, and can be integrated into larger fabricated structures—such as microcavities—to improve the collection efficiency[18,19]. A quantum dot excited on resonance by a pulsed source can have an extremely small probability of generating two photons in the same pulse—as required for this experiment. Furthermore, recent reports have indicated coherence times[20], and even time-averaged linewidths[21,22], fairly close to the radiative limit in some cases, suggesting that dephasing is slow, and thus indistinguishable photons may be achievable.

Our sample contains self-assembled InAs quantum dots (about 25 $\mu m^{-2}$) embedded in GaAs and sandwiched between distributed-Bragg-reflector (DBR) mirrors, grown by molecular-beam epitaxy[19]. Pillars (Fig. 1a) with diameters ranging from 0.3 to 5 $\mu$m and heights of 5 $\mu$m were fabricated in a random distribution by chemically assisted ion beam etching (CAIBE), using sapphire dust particles as etch masks. The resulting microcavities, exhibiting three-dimensional photon confinement, have quality factors of approximately 1,000 and measured spontaneous-emission rate enhancement (Purcell) factors as high as 5. Many pillars with only one or two quantum dots on resonance with a fundamental cavity mode were found. The sample was cooled to 3–7 K in a cryostat. To generate single photons, we focused 3-ps pulses from a Ti–sapphire laser every 13 ns onto these pillars from a steep angle. The laser was tuned to an excited-state absorption resonance of the quantum dot, typically 20–30 nm shorter in wavelength than the first-level emission wavelength. The quantum-dot emission was collected, and a single polarization was selected. The emission was then spectrally filtered with a resolution of about 0.1 nm using a diffraction grating, and coupled into a single-mode fibre.

By this method, we obtained bright, single-photon sources with excellent two-photon suppression and negligible background emission. We have chosen three quantum dots for this study, denoted as dots 1, 2 and 3, with emission wavelengths (in nm) of 931, 932 and 937, respectively. A photon-correlation measurement for dot 2 is shown in Fig. 1b. A parameter often used to quantify two-photon suppression is $g^{(2)}$, the probability of generating two photons in the same pulse, normalized by an equally bright Poisson-distributed source. We estimate $g^{(2)} = 0.053$, 0.067 and 0.071 for dots 1, 2 and 3, respectively. But for the experiment described below, the important parameter is the probability of generating two photons in the same pulse, for either of two consecutive pulses, divided by the

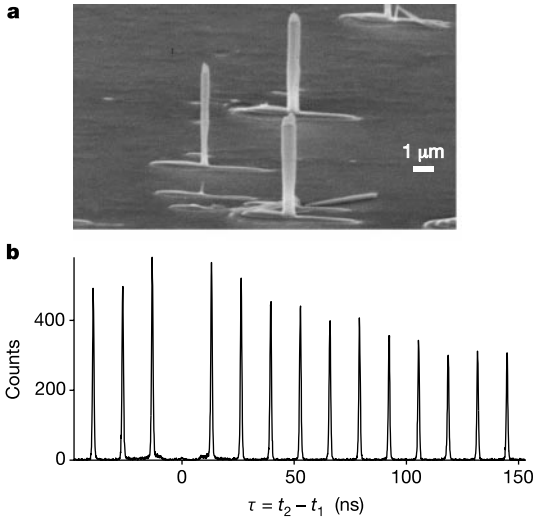


**Figure 1** The single-photon source. **a**, Pillar microcavity structures containing InAs quantum dots in a one-wavelength-thick GaAs spacer, sandwiched between distributed-Bragg-reflector (DBR) mirrors, grown by molecular-beam epitaxy. The DBR mirrors were constructed by stacking quarter-wavelength-thick GaAs and AlAs layers on top of each other. There are 12 DBR pairs above, and 30 DBR pairs below, the spacer. Pillars with diameters ranging from 0.3 to 5 $\mu$m and heights of 5 $\mu$m were fabricated in a random distribution by chemically assisted ion beam etching (CAIBE) with $Ar^+$ ions and $Cl_2$ gas, using sapphire dust particles as etch masks. Owing to the irregular shapes of the pillars, the fundamental mode is typically polarization-nondegenerate. **b**, Photon correlation histogram of emission from quantum dot 2 under pulsed, resonant excitation, obtained using a Hanbury Brown and Twiss-type set-up. The emission was split into two paths by a beam splitter, each path leading to a photon counter. A histogram was generated of the relative delay $\tau = t_2 - t_1$ between a photon detection at one counter ($t_1$) and the other ($t_2$). The vanishing central peak is the signature of suppressed two-photon emission. The parameter $g$ described in the text was obtained by dividing the area of the central peak at $\tau = 0$ by that of the nearest side peaks. The decrease of the side peaks away from $\tau = 0$ indicates blinking with a timescale of 85 ns, an effect that we usually see with resonant excitation[8]. For this measurement, the set-up shown in Fig. 3a was used, with one arm blocked.

probability of generating one photon in each pulse. We estimate this quantity to be $g = 0.039$, 0.027 and 0.025 for quantum dots 1, 2 and 3, respectively. The difference between $g^{(2)}$ and $g$ is due to blinking in our source.

Two other properties of the quantum-dot emission are also important for the two-photon interference experiment described below: the spontaneous emission lifetime and the coherence length. The average emission intensity of quantum dots 1, 2 and 3 is plotted versus time after an excitation pulse, measured under resonant excitation by a streak camera (Fig. 2a). By fitting decaying exponential functions, we estimate the spontaneous emission lifetimes $\tau_s$ of dots 1, 2 and 3 to be (in ps) 89, 166 and 351, respectively. This variation is due largely to differences in how well each quantum dot couples to its microcavity. A Michelson interferometer is used to measure the coherence length of the time-averaged emission (Fig. 2b). The curves show how the interference fringe contrast varies with path-length difference, and give the magnitude of the Fourier transform of the intensity spectra. When we did not select a single polarization, we sometimes observed oscillatory behaviour due to polarization splitting of the emission lines[23]. For dots 2 and 3 (with splittings of 13 and 17 μeV), we were able to eliminate this effect by selecting a particular linear polarization. For dot 1, the 45-μeV splitting could not easily be eliminated, probably because the quantum-dot emission couples to just one cavity mode having a polarization rotated ~45° relative to the splitting axis of the quantum dot. We estimate the 1/e coherence lengths $\tau_c$ (divided by $c$) for quantum dots 1, 2 and 3 to be (in ps) 48, 223 and 105, respectively. Quantum dot 2 is closest to being Fourier-transform-limited, with $2\tau_s/\tau_c = 1.5$. When this ratio is equal to 1, no dephasing can be present, and perfect two-photon interference is expected.

The main elements of the two-photon interference experiment are shown in Fig. 3a. The single-photon source is as described above, except that the quantum dot is excited twice every 13 ns by a pair of equally intense pulses with 2 ns separation. Two pulses, each containing zero or one photons, emerge from the single-mode fibre. They are split into two arms by a beam splitter, with one arm $(2\,\text{ns} + \Delta t)$ longer than the other. The beams then recombine at a different place on the same beam splitter. The two outputs of this interferometer are collected by photon counters, and a photon correlation histogram is generated of the relative delay time $\tau = t_2 - t_1$ for two-photon coincidence events, where $t_1$ and $t_2$ are the times at which photons are detected at detectors 1 and 2, respectively. A histogram obtained in this way for dot 2 with $\Delta t = 0$ is shown in Fig. 3b.

Five peaks appear within the central cluster, corresponding to three types of coincidence events. For peaks 1 and 5 at $\tau = \mp 4$ ns, the first photon follows the short arm of the interferometer, the second photon follows the long arm, and one photon goes to each counter. For peaks 2 and 4 at $\tau = \mp 2$ ns, both photons follow the same arm. For peak 3 at $\tau = 0$, the first photon follows the long arm, and the second photon follows the short arm, so that the two photons collide upon their second pass through the beam splitter. Only in this case can two-photon interference occur, and for perfect two-photon interference, peak 3 vanishes.

When the source successfully delivers a pair of photons, the two-

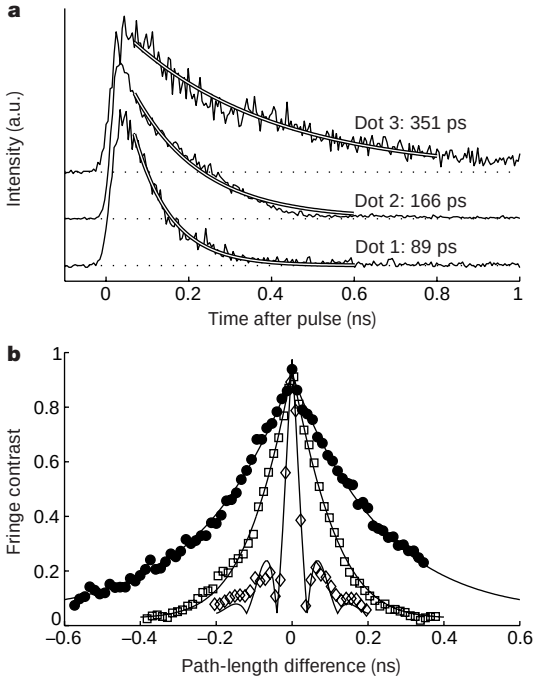


**Figure 2** Time-averaged emission properties of quantum dots 1, 2 and 3. **a**, Spontaneous emission decay under resonant excitation, measured by a streak camera. By fitting exponentials, lifetimes $\tau_s$ of 89, 166 and 351 ps for dots 1, 2 and 3, respectively, are obtained. **b**, Coherence length, measured using a Michelson interferometer, showing fringe contrast versus path-length difference. The set-up was similar to the one shown in Fig. 3a, but with the 2-ns delay removed. The fringe contrast was measured by monitoring the intensity of one of the interferometer outputs while varying one of the arm lengths over several wavelengths using a piezoelectric transducer. The arm length was then moved over long distances by a motor stage. The 1/e coherence lengths $\tau_c$ are 48, 223 and 105 ps for dots 1 (diamonds), 2 (filled circles) and 3 (squares), respectively.

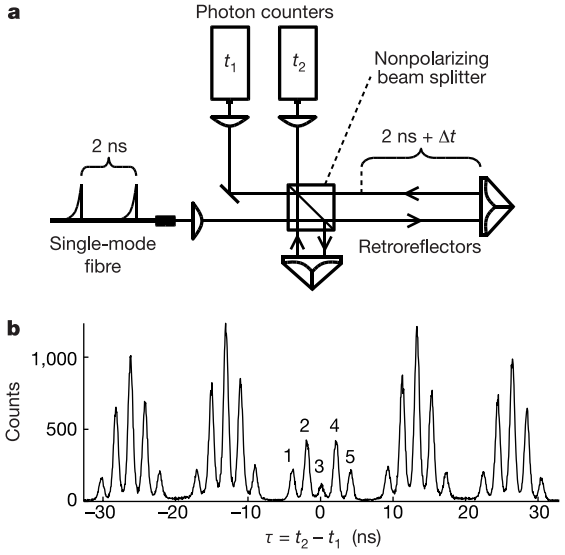


**Figure 3** Two-photon interference experiment. **a**, Every 13 ns, two pulses, separated by 2 ns and containing 0 or 1 photons, arrive through a single-mode fibre. The pulses are interfered with each other using a Michelson-type interferometer with a $(2\,\text{ns} + \Delta t)$ path-length difference. Corner-cube retroreflectors are used at the ends of the arms, so that the mode overlap is insensitive to slight angular misalignment of the optical elements. The length of the short arm can be adjusted over long distances by a 15-cm motor stage. The fringe contrast measured using a laser with a long coherence length was 0.92, limited by optical surface imperfections. The interferometer outputs are collected by photon counters, and the resulting electronic signals are correlated using a time-to-amplitude converter followed by a multi-channel analyser card, which generates a histogram of the relative delay time $\tau = t_2 - t_1$ between a photon detection at one counter ($t_1$) and the other ($t_2$). **b**, Such a histogram (53-ps bin size) obtained for quantum dot 2, with $\Delta t = 0$. The number of repetitions was $N = 2.3 \times 10^{10}$ (5 min), and the combined two-photon generation and detection efficiency was $\eta^{(2)} = 2.5 \times 10^{-6}$, which includes all losses in the experimental set-up. The small area of peak 3 demonstrates two-photon interference.

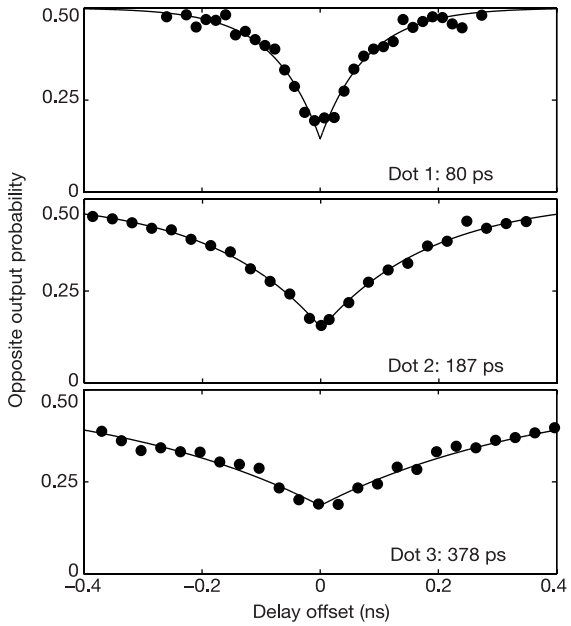


**Figure 4** The probability that two photons that collide at the beam splitter leave in opposite directions, plotted as a function of interferometer delay offset, $\Delta t$. Data are shown for quantum dots 1, 2 and 3. The drops in the coincidence rate near zero offset demonstrate two-photon interference. From model fits (solid lines), the 1/e widths of the dips are estimated as 80, 187 and 378 ps for dots 1, 2 and 3, respectively, in close agreement with the measured spontaneous emission lifetimes.

photon state can be written as

$$|\psi\rangle = \int \mathrm{d}s\, x(s) \int \mathrm{d}t\, y(t) a^{\dagger}(s) a^{\dagger}(t + 2\,\mathrm{ns})|0\rangle \qquad (1)$$

where $a^{\dagger}(t)$ is the photon creation operator at time $t$, $x(s)$ and $y(t)$ define the photon wave packets, and $|0\rangle$ is the vacuum state. We assume that the photon wave packets are much shorter than 2 ns. In the limit of low collection efficiency, the mean areas of peaks 1–5 are

$$A_1 = N\eta^{(2)} R^3 T,\ A_2 = N\eta^{(2)}[R^3 T(1+2g) + RT^3]$$

$$A_3 = N\eta^{(2)}[(R^3 T + RT^3)(1+2g) - 2(1-\varepsilon)^2 R^2 T^2 V(\Delta t)] \qquad (2)$$

$$A_4 = N\eta^{(2)}[R^3 T + RT^3(1+2g)],\ A_5 = N\eta^{(2)} RT^3$$

where $N$ is the number of repetitions, $\eta^{(2)}$ is the combined two-photon generation and detection efficiency, and $R$ and $T$ are the beam-splitter intensity coefficients of reflection and transmission, respectively. As defined above, the parameter $g$ characterizes the two-photon emission probability, with $g = 0$ for an ideal single-photon source, and $g = 1$ for a Poisson-distributed source (without blinking). The parameter $1 - \varepsilon$ is the interference fringe contrast measured when an ideal monochromatic calibration source is sent into the interferometer, and accounts for optical surface imperfections. The parameter $V(\Delta t) = \langle |\int \mathrm{d}t\, x(t) y^{*}(t + \Delta t)|^2 \rangle$ in the expression for peak 3 is the mean overlap between the wave packets of the two photons for interferometer path-length difference $(2\,\mathrm{ns} + \Delta t)$. An ensemble average is performed over all possible two-photon states generated by the source.

The signature of two-photon interference that we observe is the small size of peak 3 in Fig. 3b, compared with peaks 2 and 4. We define the quantity $M(\Delta t) = A_3/(A_2 + A_4)$ in terms of the peak areas in equation (2). This quantity is equal to the conditional probability, given that two photons collide at the beam splitter, that the photons leave in opposite directions, in the limit $g \approx 0$. We measured $M(\Delta t)$ while varying the interferometer path length offset $\Delta t$ (Fig. 4). For all three quantum dots, we observe reductions in the coincidence probability near $\Delta t = 0$, by factors of 0.61, 0.69 and 0.62 for dots 1, 2 and 3, respectively. The remaining coincidences we see are partly due to independently measured optical imperfections in our set-up, $R/T = 1.1$ and $(1 - \varepsilon) = 0.92$. Without these imperfections, the coincidence reduction factors would be $V(0) = 0.72$, 0.81 and 0.74 for quantum dots 1, 2 and 3, respectively.

Table 1 **Summary of quantum-dot parameters**

| | $g^{(2)}$ | $g$ | $\tau_s$ (ps) | $\tau_c$ (ps) | $\tau_m$ (ps) | $V(0)$ |
|---|---|---|---|---|---|---|
| Dot 1 | 0.053 | 0.039 | 89 | 48 | 80 | 0.72 |
| Dot 2 | 0.067 | 0.027 | 166 | 223 | 187 | 0.81 |
| Dot 3 | 0.071 | 0.025 | 351 | 105 | 378 | 0.74 |

For the three quantum dots chosen for this study, we show the conventional two-photon suppression parameter $g^{(2)}$, the ratio $g$ of the probability of emitting two photons in either of two consecutive pulses to the probability of emitting one photon in each pulse, the spontaneous emission lifetime $\tau_s$, the coherence length $\tau_c$, the 1/e width of the Mandel dip $\tau_m$, and the two-photon overlap at zero path-length difference $V(0)$.

To analyse these data, we fitted the function $M(\Delta t) = 0.5[1 - a\exp(-|\Delta t|/\tau_m)]$, where the fitting parameters $a$ and $\tau_m$ characterize the depth and the width of the coincidence dip, respectively. The fits, shown as solid lines in Fig. 4, match the data well. For an ideal spontaneous-emission source, with instantaneous initial excitation and no decoherence, $a$ would differ from 1 only because of imperfections in the optical set-up, and $\tau_m$ would be equal to the spontaneous emission lifetime. The fitted values of $\tau_m$ we obtain (in ps) are 80, 187 and 378 for quantum dots 1, 2 and 3, respectively. These values agree quite well with the spontaneous emission decay lifetimes $\tau_s$ obtained in Fig. 2a (see also Table 1). For quantum dots 1 and 3, this result is surprising, given the short coherence lengths $\tau_c$ listed above. We conclude that, for quantum dots 1 and 3, the primary spectral broadening mechanism occurs on a timescale much longer than 2 ns. Such a 'spectral diffusion' effect could occur owing to charge fluctuations in the vicinity of the quantum dot, for example[22].

For quantum dot 2, we calculate a mean two-photon overlap of at least 0.81. The remaining imperfection could arise from several decoherence mechanisms. When the quantum dot is first excited by a laser pulse, the generated electron–hole pair is initially in an excited state, and must relax to its lowest state through phonon emission before a photon can be emitted at the proper wavelength. The ratio of this relaxation time, which could be as long as tens of picoseconds, to the lowest-state radiative lifetime could limit the performance of this source. Decoherence by phonons[24,25] is another possible mechanism, though we see little temperature dependence from 3 to 7 K. Finally, the spectral diffusion mechanism noted above could also potentially contribute to decoherence on short timescales.

The two-photon interference effect that we observe indicates a large enough degree of photon indistinguishability to perform interesting quantum-optical experiments. The performance of most schemes based on two-photon interference depends on the same wave-packet overlap as measured here. For example, for a single-photon implementation of a scheme to generate single pairs of polarization-entangled photons[17], the polarization correlation would ideally be unity in the horizontal/vertical basis, and 0.81 in the +45°/−45° basis, violating Bell's inequality. We hope that other applications, such as quantum teleportation and quantum logic gates, will become feasible as the performance of single-photon sources continues to improve. □

Received 27 June; accepted 23 August 2002; doi:10.1038/nature01086.

1. De Martini, F., Di Giuseppe, G. & Marrocco, M. Single-mode generation of quantum photon states by excited single molecules in a microcavity trap. *Phys. Rev. Lett.* **76,** 900–903 (1996).
2. Brunel, C., Lounis, B., Tamarat, P. & Orrit, M. Triggered source of single photons based on controlled single molecule fluorescence. *Phys. Rev. Lett.* **83,** 2722–2725 (1999).
3. Lounis, B. & Moerner, W. E. Single photons on demand from a single molecule at room temperature. *Nature* **407,** 491–493 (2000).

  

4. Kim, J., Benson, O., Kan, H. & Yamamoto, Y. A single-photon turnstile device. *Nature* **397,** 500–503 (1999).
5. Beveratos, A. *et al.* Room temperature stable single-photon source. *Eur. Phys. J. D* **18,** 191–196 (2002).
6. Kuhn, A., Hennrich, M. & Rempe, G. Deterministic single-photon source for distributed quantum networking. *Phys. Rev. Lett.* **89,** 067901 (2002).
7. Michler, P. *et al.* A quantum dot single-photon turnstile device. *Science* **290,** 2282–2285 (2000).
8. Santori, C., Pelton, M., Solomon, G., Dale, Y. & Yamamoto, Y. Triggered single photons from a quantum dot. *Phys. Rev. Lett.* **86,** 1502–1505 (2001).
9. Zwiller, V. *et al.* Single quantum dots emit single photons at a time: antibunching experiments. *Appl. Phys. Lett.* **78,** 2476–2478 (2001).
10. Yuan, Z. *et al.* Electrically driven single photon source. *Science* **295,** 102–105 (2002).
11. Gérard, J.-M. & Gayral, B. Strong Purcell effect for InAs quantum boxes in three-dimensional solid-state microcavities. *J. Lightwave Technol.* **17,** 2089–2095 (1999).
12. Knill, E., Laflamme, R. & Milburn, G. J. A scheme for efficient quantum computation with linear optics. *Nature* **409,** 46–52 (2001).
13. Fearn, H. & Loudon, R. Theory of two-photon interference. *J. Opt. Soc. Am. B* **6,** 917–927 (1989).
14. Hong, C. K., Ou, Z. Y. & Mandel, L. Measurement of subpicosecond time intervals between two photons by interference. *Phys. Rev. Lett.* **59,** 2044–2046 (1987).
15. Bennett, C. H. & Brassard, G. *Proc. IEEE Int. Conf. on Computers, Systems and Signal Processing* 175–179 (IEEE, New York, 1984).
16. Bouwmeester, D., Ekert, A. & Zeilinger, A. *The Physics of Quantum Information* 49–92 (Springer, Berlin, 2000).
17. Shih, Y. H. & Alley, C. O. New type of Einstein–Podolsky–Rosen–Bohm experiment using pairs of light quanta produced by optical parametric down conversion. *Phys. Rev. Lett.* **61,** 2921–2924 (1988).
18. Moreau, E. *et al.* Single-mode solid-state single photon sources based on isolated quantum dots in pillar microcavities. *Appl. Phys. Lett.* **79,** 2865–2867 (2001).
19. Solomon, G. S., Pelton, M. & Yamamoto, Y. Single-mode spontaneous emission from a single quantum dot in a three-dimensional microcavity. *Phys. Rev. Lett.* **86,** 3903–3906 (2001).
20. Borri, P. *et al.* Ultralong dephasing time in InGaAs quantum dots. *Phys. Rev. Lett.* **87,** 157401 (2001).
21. Gammon, D., Snow, E. S., Shanabrook, B. V., Katzer, D. S. & Park, D. Homogeneous linewidths in the optical spectrum of a single gallium arsenide quantum dot. *Science* **273,** 87–90 (1996).
22. Bayer, M. & Forchel, A. Temperature dependence of the exciton homogeneous linewidth in $In_{0.60}Ga_{0.40}As/GaAs$ self-assembled quantum dots. *Phys. Rev. B* **65,** 041308(R) (2002).
23. Kulakovskii, V. D. *et al.* Fine structure of biexciton emission in symmetric and asymmetric CdSe/ZnSe single quantum dots. *Phys. Rev. Lett.* **82,** 1780–1783 (1999).
24. Besombes, L., Kheng, K., Marsal, L. & Mariette, H. Acoustic phonon broadening mechanism in single quantum dot emission. *Phys. Rev. B* **63,** 155307 (2001).
25. Fan, X., Takagahara, T., Cunningham, J. E. & Wang, H. Pure dephasing induced by exciton–phonon interactions in narrow GaAs quantum wells. *Solid State Commun.* **108,** 857–861 (1998).


**Acknowledgements** We thank A. Scherer and T. Yoshie for access to the CAIBE system and for their help in fabrication of the structures; J. Plant for assistance with SEM imaging; and B. C. Sanders for discussions. This work was supported in part by MURI; G.S.S. was supported by DARPA, ARO and JST.

**Competing interests statement** The authors declare that they have no competing financial interests.

**Correspondence** and requests for materials should be addressed to C.S. (e-mail: chars@stanford.edu).

# Superconductivity in compressed lithium at 20 K

**Katsuya Shimizu*†, Hiroto Ishikawa*, Daigoroh Takao*, Takehiko Yagi‡ & Kiichi Amaya*†**

** Department of Physical Science, Graduate School of Engineering Science; and † Research Center for Materials Science at Extreme Conditions, Osaka University, Toyonaka, Osaka 560-8531, Japan*
*‡ The Institute for Solid State Physics, University of Tokyo, Kashiwa-shi, chiba 277-8581, Japan*

**Superconductivity at high temperatures is expected in elements with low atomic numbers, based in part on conventional BCS (Bardeen–Cooper–Schrieffer) theory[1]. For example, it has been predicted that when hydrogen is compressed to its dense metallic phase (at pressures exceeding 400 GPa), it will become superconducting with a transition temperature above room temperature[2]. Such pressures are difficult to produce in a laboratory setting, so the predictions are not easily confirmed. Under normal conditions lithium is the lightest metal of all the elements, and may become superconducting at lower pressures[3,4]; a tentative observation of a superconducting transition in Li has been previously reported[5]. Here we show that Li becomes superconducting at pressures greater than 30 GPa, with a pressure-dependent transition temperature ($T_c$) of 20 K at 48 GPa. This is the highest observed $T_c$ of any element; it confirms the expectation that elements with low atomic numbers will have high transition temperatures, and suggests that metallic hydrogen will have a very high $T_c$. Our results confirm that the earlier tentative claim[5] of superconductivity in Li was correct.**

Previous theory[6] has predicted that dense Li will undergo a new structural transition towards a 'paired-atom' phase at pressures near

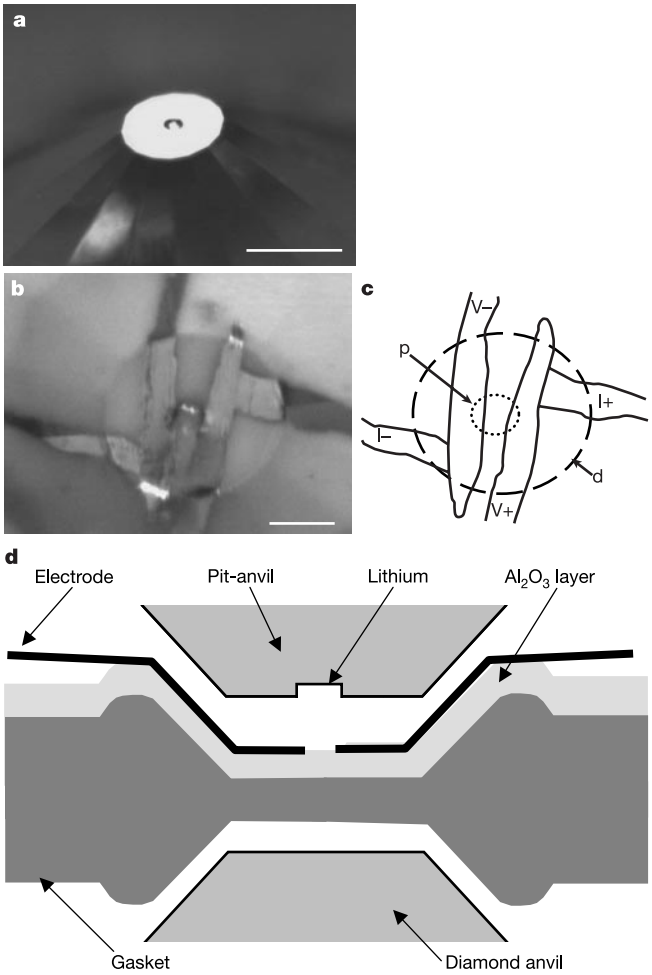


**Figure 1** Arrangement of sample and electrodes on the diamond anvils. **a**, Photograph of a pit, 50 μm in diameter and 7 μm deep, on the 300-μm pressure surface of the synthetic type Ib diamond anvil. The pit was prepared by a focused ultraviolet beam from pulsed KrF-excimer laser, wavelength 248 nm. Scale bar, 0.3 mm. **b**, Electrodes on a thin aluminium oxide layer. Two platinum-film electrodes, 5-μm thick, are placed to touch the sample in the pit; scale bar, 0.1 mm. **c**, Schematic drawing of **b**. A quasi-four-wire electrical resistance measurement was performed. The measured resistivity included one of the platinum films which were placed in series connecting to the sample in the pit (p) on the diamond-anvil surface (d). A direct current of 1 mA is applied through I+ to I−, and the voltage drop between V+ and V− is recorded. **d**, Schematic drawing of the cross-section of our set-up at the top of the diamonds anvils. Ruby chips are located the bottom of the pit; the pressure was controlled by helium gas, and determined by a conventional ruby-fluorescence method through the optical windows of the cryostat.